PHYSICS OF PLASMAS **12**, 014501 (2005)

Enhanced Landau damping of finite amplitude electrostatic waves in the presence of suprathermal electron tails

D. V. Rose[a)]
Mission Research Corporation, Albuquerque, New Mexico 87110

J. Guillory and J. H. Beall[b)]
School of Computational Sciences, George Mason University, Fairfax, Virginia 22030

(Received 5 April 2004; accepted 23 September 2004; published online 3 December 2004)

Increased Landau damping of electrostatic waves in the presence of low density suprathermal electron populations is examined. An electrostatic dispersion analysis is compared directly with one-dimensional particle-in-cell simulations of the Landau damping rates. An analytic damping rate formula is presented that is in good agreement with numerical solutions of the dispersion equation over a range of parameters. © *2005 American Institute of Physics*. [DOI: 10.1063/1.1818697]

Landau damping[1] is a collisionless process that acts to damp electrostatic waves in a plasma. In many physical situations such as electron and laser beam propagation in dense plasmas, hot low-density electron populations can be generated (see, for example, Refs. 2–9). The presence of such low-density electron distributions can act to increase the magnitude of the electrostatic wave damping rate. This paper investigates this effect by examining numerical solutions of the plasma dispersion equation and comparing the calculated damping rates to one-dimensional (1D) particle-in-cell (PIC) simulations.

In addition to the plasma configurations studied here, enhanced Landau damping of electrostatic plasma waves has been identified for sinusoidally modulated plasma densities.[10] This situation can arise in strongly driven laser plasmas. In contrast, the reduction of Landau damping rates in strongly non-Maxwellian plasmas have been studied for the case of laser-heated plasmas.[11]

The total electron velocity distribution function used in this work is given by the sum of a fractional f "hot" Maxwellian distribution and a "cold" bulk distribution;

$$f_e(v) \propto (1-f)\left(\frac{1}{T_c}\right)^{3/2} v^2 \exp\left(-\frac{av^2}{T_c}\right) + f\left(\frac{1}{T_h}\right)^{3/2} v^2 \exp\left(-\frac{av^2}{T_h}\right). \quad (1)$$

Here, T_h and T_c are the hot and cold electron temperatures and $a=m/2k_B$, where m is the electron mass and k_B is the Boltzmann constant. The total electron density is the sum of the hot and cold electron population densities. A sample electron speed distribution function is plotted in Fig. 1 showing the sum of a 1% Maxwellian distribution at 10 eV added to a 1 eV Maxwellian distribution. We note that other analytic forms have been used to model a hot electron tail population including Lorenztian distributions[12,13] and "super-Gaussian" distributions.[8]

[a)]Electronic mail: drose@mrcabq.com
[b)]Also at St. John's College, Annapolis, MD 21401 and E. O. Hulburt Center for Space Sciences, Naval Research Laboratory, Washington, DC 20375.

The 1D PIC simulations were carried out using the LSP code[14] with an electrostatic field solver. Both periodic and bounded simulation conditions were used and the length of the simulation region was 1 to 100 times the wavelength under investigation. Typically >200 particles per cell were used to provide a reasonable representation of the electron and ion velocity distributions.

The electrostatic wave damping rates are determined from the dielectric function

$$\epsilon(\omega,k) = 1 + \sum_{j=i,c,h} \chi_j(\omega,k), \quad (2)$$

where χ_j is the susceptibility of each species (i=ion, c=cold electron, h=hot electron species, respectively), given by

$$\chi_j(\omega,k) = -\frac{\omega_j^2}{2v_j^2k^2} Z'\left(\frac{\omega}{\sqrt{2}v_jk}\right). \quad (3)$$

Here, Z is the plasma dispersion function and

$$Z'(A) = -2[1 + AZ(A)].$$

v_j is the thermal speed by species, $\omega_j=\sqrt{n_je^2/m_j\epsilon_0}$, where n_j is the number density of species j and ϵ_0 is the permittivity. (We note that similar kinetic treatments for the case of multiple ion populations can be found in Refs. 15 and 16.) Here, the complex roots of

$$\epsilon(\omega,k) = 0 \quad (4)$$

are found numerically or using analytic treatments in the zero amplitude limit, as given below.

Defining $n_c=n_p(1-f)$ and $n_h=n_pf$, the Debye lengths for the cold and hot electron populations are written as $\lambda_D^2 = T_c/4\pi n_pe^2$ and $\lambda_{Dh}^2=T_h/4\pi n_pfe^2$, respectively. Neglecting the contributions from the ion term Eq. (4), the dispersion for the hot and cold electron species can be written as

$$D_r(\Omega) + iD_i(\Omega) = 0, \quad (5)$$

where the real and imaginary terms are

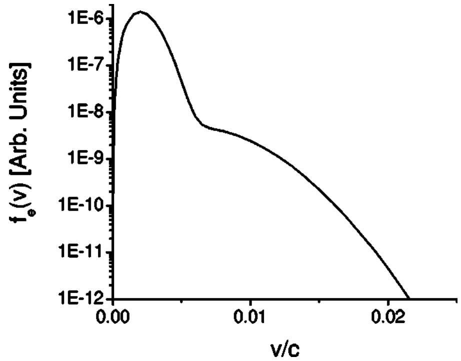

FIG. 1. Sample electron speed distribution function for $f=0.01$, $T_c=1$ eV, and $T_h=10$ eV.

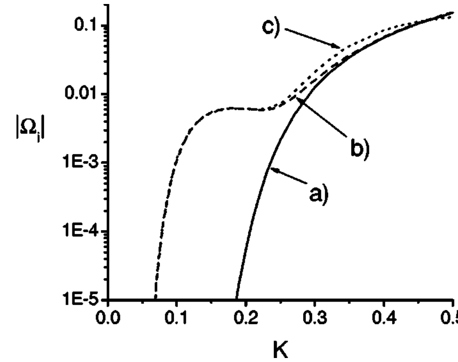

FIG. 2. Numerical solutions of damping rates for (a) one-electron temperature dispersion relation and (b) two-electron temperature dispersion relation for $f=0.01$, $T_c=1$ eV, and $T_h=10$ eV. The analytic solution for the two temperature damping rate, Eq. (16), is shown in (c).

$$D_r(\Omega) = 1 - \sum_{n=1}^{\infty} A_n B_n \frac{K^{2n-2}}{\Omega^{2n}} \tag{6}$$

and

$$D_i(\Omega) = \left(\frac{\pi}{2}\right)^{1/2} \frac{\Omega}{K^3}\left[(1-f)\exp\left(-\frac{\Omega^2}{2K^2}\right) + f\left(\frac{T_c}{T_h}\right)^{3/2}\exp\left(-\frac{\Omega^2}{2K^2}\frac{T_c}{T_h}\right)\right], \tag{7}$$

respectively. Here, $\Omega=\omega/\omega_p$, $K=k\lambda_D$, and

$$A_n = \prod_{i=1}^{n}[2n-(2i-1)], \tag{8}$$

$$B_n = 1 - f + f\left(\frac{T_h}{T_c}\right)^{n-1}. \tag{9}$$

The solution of

$$D_r(\Omega_r) = 0 \tag{10}$$

gives the real frequency Ω_r of the wave and the damping rate is determined from

$$\Omega_i \simeq - \left.\frac{D_i}{\partial D_r/\partial\Omega}\right|_{\Omega_r}. \tag{11}$$

The real frequency can be approximated by solving the equation (containing only two terms for algebraic tractability)

$$0 \simeq 1 - A_1B_1\frac{1}{\Omega_0^2} - A_2B_2\frac{K^2}{\Omega_0^4}. \tag{12}$$

The solution is then (using the positive root)

$$\Omega_0 \simeq \sqrt{\frac{1}{2}+\frac{1}{2}(1+12K^2B_2)^{1/2}}. \tag{13}$$

For the determination of the imaginary frequency, Eq. (7), we evaluate $\partial D/\partial\Omega$ at Ω_0. The result is

$$\left.\frac{\partial D_r}{\partial \Omega}\right|_{\Omega_0} \simeq \frac{2}{\Omega_0^3} + 12\frac{B_2K^2}{\Omega_0^5} + 90\frac{B_3K^4}{\Omega_0^7} \tag{14}$$

and substitution of this expression into Eq. (11) gives

$$\Omega_i \simeq \sqrt{\frac{\pi}{8}}\frac{1}{K^3}\left[(1-f)\exp\left(-\frac{\Omega_0^2}{2K^2}\right) + f\left(\frac{T_c}{T_h}\right)^{3/2}\exp\left(-\frac{\Omega_0^2}{2K^2}\frac{T_c}{T_h}\right)\right] \times \Omega_0^8(\Omega_0^4 + 6B_2K^2\Omega_0^2 + 45B_3K^4)^{-1}. \tag{15}$$

Noting that in the limit $12K^2B_2 \ll 1$, $\Omega_0 \simeq \sqrt{1+3K^2B_2}$, the damping rate can be further approximated as

$$\Omega_i \simeq -\sqrt{\frac{\pi}{8}}\frac{1}{K^3}\left[(1-f)\exp\left(-\frac{1}{2K^2}-\frac{3}{2}B_2\right) + f\left(\frac{T_c}{T_h}\right)^{3/2}\exp\left(-\frac{T_c}{2K^2T_h}-\frac{3}{2}\frac{T_c}{T_h}B_2\right)\right]. \tag{16}$$

The derivation of this expression is discussed in Ref. 9, but the final equation is incorrect as written there.

It has been pointed out elsewhere that the finite number of terms carried in the expansions (including those used here) can lead to errors in the magnitude of damping rate for some parameter ranges.[17] However, the resulting closed form solution as presented here provides considerable insight into the role of the hot electron population on the damping rate as will be shown below. For finite amplitude oscillations, such as those treated in the PIC simulations discussed below, we note that correction terms can be added to the zero amplitude model (see, for example, Ref. 18).

Equation (16) is compared with the numerical solution of Eq. (4) in Fig. 2. Equation (16) overestimates the numerical solutions for $K \gtrsim 0.3$, but overall agreement is found over a range of K for the selected parameters.

As illustrated in Fig. 2, the addition of a small hot electron population significantly increases the damping rates at smaller K values. We note that similar enhanced damping rates at small K were found for the specific case of spatially modulated plasma densities in Ref. 10. For larger hot fractions the enhanced damping effect is even greater, especially for $K \lesssim 0.35$. This is illustrated in Fig. 3(c) for $T_c=1$ eV, $T_h=10$ eV, and $f=0.1$. The discrepancy between the numerical solution of Eq. (4) and Eq. (16) for $K \gtrsim 0.15$ is larger than

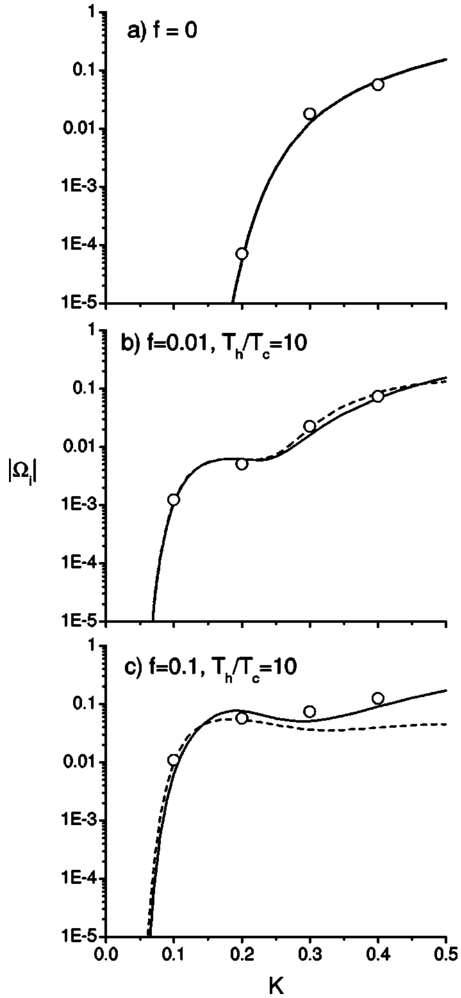

FIG. 3. Comparison of damping rate magnitudes with 1D PIC simulations (open circles). The solid lines are numerical solutions to the dispersion relation, Eq. (4), and the dashed lines are from Eq. (16). (a) $f=0$, $T_h=0$, (b) $f=0.01$, $T_c=1$ eV, and $T_h=10$ eV and (c) $f=0.1$, $T_c=1$ eV, and $T_h=10$ eV.

the $f=0.01$ case because the parameter $3K^2B_2$ in the expansion of the real part of the dielectric function now exceeds the limit of being a small parameter.

The PIC simulation results shown in Fig. 3 support the overall trends of enhanced damping rates to the extent that a linear damping rate can be obtained. For larger damping rate

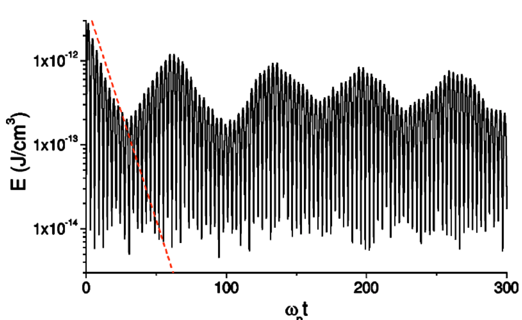

FIG. 4. (Color online). Total electrostatic wave energy from a 1D PIC simulation with $K=0.2$, $f=0.1$, $T_c=1$ eV, $T_h=10$ eV, and $n_p=10^9$ cm^{-3}. The dashed line shows the fit used to determine the linear damping rate plotted in Fig. 3(c).

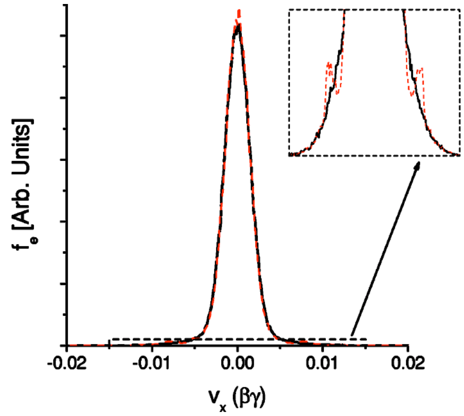

FIG. 5. (Color online). Electron v_x distribution function at 0 (solid) and 25 (dashed) plasma periods for the simulation parameters of Fig. 4. The inset plot details the small amplitude portion of the distribution function.

magnitudes, the duration of the linear stage is often very brief, e.g., of order 10 plasma periods or less. For finite amplitude initial plasma oscillations, nonlinear effects dominate for $\epsilon > \epsilon^*$, where $\epsilon = K\sqrt{W}$, W is the dimensionless wave energy density and ϵ^* is the initial wave amplitude that denotes the transition between the linear and nonlinear regimes,[19,20] which can be approximated as $\epsilon^* \sim \Omega_i^2/\sqrt{2}$. Above this transition value, the asymptotic behavior of the oscillations can become the more relevant feature. This is illustrated in Fig. 4, which plots the total electrostatic wave energy density from a PIC simulation as a function of time for $K=0.2$, $f=0.1$, and $T_h/T_c=10$. The linear stage of the damping corresponds to the first $\sim$10 oscillations and the linear damping rate is approximately given by the dashed line in Fig. 4. For this example, the initial wave energy density W is $\sim$0.023, which is much greater than the transition wave energy amplitude $\simeq \Omega_i^4/2K^2 \sim 4\times 10^{-4}$.

The electron distribution from this simulation, shown in Fig. 5, indicates that the damping occurs at the phase velocity Ω_0/k as expected. For large initial wave amplitudes, the simulations show the formation of a plateau in the distribution function for velocity magnitudes greater than this phase velocity, consistent with quasilinear models[21] and other finite amplitude simulations.[20,22,23]

The enhancement of collisionless Landau damping in the presence of low density suprathermal electron distributions has been examined via numerical solutions of the plasma dispersion function and 1D PIC simulations. A closed-form solution of the dispersion relation has been developed that characterizes the electron distribution in terms of f and T_h/T_c. Direct comparisons with numerical solutions of the dispersion relation show the closed-form solution captures the correct overall behavior of the damping rate. The 1D PIC simulations further support the dispersion relation calculations and lend credence to the PIC methodology being applied to more dynamic and complex physical situations involving collisionless plasmas.

ACKNOWLEDGMENTS

The authors thank Dr. T. C. Genoni, Mission Research Corporation (MRC) for helpful discussions of the dispersion relation solutions, and R. E. Clark and Dr. D. R. Welch, also at MRC, for discussions on plasma simulation and the LSP code.

[1]L. Landau, J. Phys. (USSR) **10**, 45 (1946).
[2]K. Papadopoulos and T. Coffey, J. Geophys. Res. **79**, 674 (1974).
[3]H. Freund, R. A. Smith, K. Papadopoulos, and P. Palmadesso, Phys. Fluids **24**, 442 (1981).
[4]M. Tanaka and K. Papadopoulos, Phys. Fluids **26**, 1697 (1983).
[5]H. Rowland, J. Geophys. Res. **93**, 12916 (1988).
[6]J. G. Wang, D. L. Newman, and M. V. Goldman, J. Atmos. Sol.-Terr. Phys. **59**, 2461 (1997).
[7]A. F. Vinas, H. K. Wong, and A. J. Klimas, Astrophys. J. **528**, 509 (2000).
[8]E. Fourkal, V. Y. Bychenkov, W. Rozmus, R. Sydora, C. Kirby, C. E. Capjack, S. H. Glenzer, and H. A. Baldis, Phys. Plasmas **8**, 550 (2001).
[9]D. V. Rose, J. U. Guillory, and J. H. Beall, Phys. Plasmas **9**, 1000 (2002).
[10]M. Curtet and G. Bonnaud, Phys. Rev. E **60**, 5052 (1999).
[11]B. B. Afeyan, A. E. Chou, J. P. Matte, R. P. J. Town, and W. J. Kruer, Phys. Rev. Lett. **80**, 2322 (1998).
[12]R. M. Thorne and D. Summers, Phys. Fluids B **3**, 2117 (1991).
[13]D. Summers and R. M. Thorne, Phys. Fluids B **3**, 1835 (1991).
[14]LSP is a software product of Mission Research Corporation, Albuquerque, NM 87110 (http://www.mrcabq.com).
[15]H. X. Vu, J. M. Wallace, and B. Bezzerides, Phys. Plasmas **1**, 3542 (1994).
[16]E. A. Williams, R. L. Berger, R. P. Drake, A. M. Rubenchik, B. S. Bauer, D. D. Meyerhofer, A. C. Gaeris, and T. W. Johnston, Phys. Plasmas **2**, 129 (1995).
[17]C. J. McKinstrie, R. E. Giacone, and E. A. Startsev, Phys. Plasmas **6**, 463 (1999).
[18]V. N. Tsytovich, *Nonlinear Effects in Plasma* (Plenum, New York, 1970).
[19]T. O'Neil, Phys. Fluids **8**, 2255 (1965).
[20]M. Brunetti, F. Califano, and F. Pegoraro, Phys. Rev. E **62**, 4109 (2000).
[21]A. A. Vedenov, in *Review of Plasma Physics*, edited by M. A. Leontovich (Consultants Bureau, New York, 1967), Vol. 3, pp. 243–253.
[22]R. E. Giacone and H. X. Vu, Phys. Plasmas **5**, 1455 (1998).
[23]H. X. Vu, D. F. DuBois, and B. Bezzerides, Phys. Rev. Lett. **86**, 4306 (2001).